Arabian Journal of Chemistry (2023) **16**, 105089

King Saud University

Arabian Journal of Chemistry

www.ksu.edu.sa
www.sciencedirect.com

ORIGINAL ARTICLE

Bioassay-guided identification of potential Alzheimer's disease therapeutic agents from Kaempferol-Enriched fraction of *Aframomum melegueta* seeds using *in vitro* and chemoinformatics approaches

Ifeoma Felicia Chukwuma [a,b,*], Timothy Prince Chidike Ezeorba [a,b,c], Florence Nkechi Nworah [a], Victor Onukwube Apeh [d], Mohammad Khalid [e], Sherouk Hussein Sweilam [e,f]

[a] *Department of Biochemistry, Faculty of Biological Sciences, University of Nigeria, Enugu State 410001, Nigeria*
[b] *Department of Genetics and Biotechnology, Faculty of Biological Sciences, University of Nigeria, Enugu State 410001, Nigeria*
[c] *Department of Molecular Biotechnology, School of Biosciences, University of Birmingham Edgbaston, Birmingham B15 2TT, United Kingdom*
[d] *Federal College of Dental Technology and Therapy, Enugu, Department of Applied Sciences, Enugu 01473, Nigeria*
[e] *Department of Pharmacognosy, College of Pharmacy, Prince Sattam Bin Abdulaziz University, Al-Kharj 11942, Saudi Arabia*
[f] *Department of Pharmacognosy, Faculty of Pharmacy, Egyptian Russian University, Cairo-Suez Road, Badr City, Cairo 11829, Egypt*

Received 25 February 2023; accepted 15 June 2023
Available online 21 June 2023

KEYWORDS

Aframomum melegueta;
Acetylcholinesterase;
Antioxidants;
Butyrylcholinesterase;
Drug-likeness

Abstract Alzheimer's disease (AD) has become a major public health concern and the fifth major cause of death among the aging population globally. In this study, the total phenols and flavonoids contents (TPC and TFC) and *in vitro* antioxidant actions of the methanol extract and the various fractions of *Aframomum melegueta* were evaluated using 2,2-diphenyl-2-picrylhydrazyl (DPPH) radical scavenging activity, nitric oxide scavenging activity (NO), lipid peroxidation (TBARS) activity and ferric reducing power assay (FRAP). Furthermore, acetylcholinesterase (AChE) and butyrylcholinesterase (BuChE) inhibitory activities of the two most potent fractions were

* Corresponding author at: Department of Biochemistry, Faculty of Biological Sciences, University of Nigeria, Enugu State 410001, Nigeria.
E-mail addresses: chukwuma.ifeoma@unn.edu.ng (I.F. Chukwuma), timothy.ezeorba@unn.edu.ng (T.P.C. Ezeorba), florence.nworah@unn.edu.ng (F.N. Nworah), victorapeh@gmail.com (V.O. Apeh), drkhalid8811@gmail.com (M. Khalid), s.sweilam@psau.edu.sa (S.H. Sweilam).
Peer review under responsibility of King Saud University.

Production and hosting by Elsevier

https://doi.org/10.1016/j.arabjc.2023.105089

investigated, and the phytochemicals identified in the ethyl acetate fraction, which had the best antioxidant and cholinesterase inhibitory effects were subjected to chemoinformatics studies. The extract and its fraction had high amounts of TPC and TFC. The ethyl acetate fraction exerted the best DPPH, NO, TBARS, and FRAP inhibition with IC_{50} values of 5.06, 6.58, 2.12, and 88.73 μg/mL, respectively. Interestingly, n-hexane and ethyl acetate fractions inhibited AChE (IC_{50}16.83 and 11.67 μg/mL) and BuChE (IC_{50} 7.54 and 5.21 μg/mL) enzymatic activities more than the standard inhibitor, rivastigmine which had 11.99 and 11.40 μg/mL IC_{50} values, respectively. A total of 18 compounds were identified in ethyl acetate fraction, and kaempferol was the major component, with 40.01 μg/g (30%). More strikingly, the top-scoring compounds (catechin, and kaempferol) exhibited good binding affinity, and interacted favorably with amino acids residues around and within the active sites of AChE and BuChE and also obeyed drug-likeness rules, and did not show a tendency towards toxicity when placed side by side with rivastigmine which is immunogenic. Thus, *A. melegueta* seeds contain safe bioactive chemicals, which could be a veritable remedy for managing Alzheimer's and other neurodegenerative diseases.

1. Introduction

The global increase in life expectancy mediated by advancement in medical care, improved sanitation, and health management awareness has increased the aging population (Mangmool et al., 2021). Regrettably, this progress has not been translated to the well-being of the elderly (Kpemissi et al., 2023). The greatest challenge now lies in homeostatic imbalance and physiological malfunction among the elderly leading to age-related diseases including metabolic syndrome, cardiovascular, atherosclerosis, and neurodegenerative diseases (Mangmool et al., 2021). The prime accelerator of the pathophysiology of these diseases is mainly a result of cellular and organ damage, which is the hallmark of disruption of redox equilibrium. Excessive generation of reactive oxygen and reactive nitrogen species (ROS and RNS) such as superoxide radical anion (O_2^-), hydroxyl radical (HO–), hydrogen peroxide (H_2O_2), peroxynitrite (ONOO–), and nitric oxide (NO), from endogenous and exogenous sources, usually overwhelms the functionality and expression of the body's antioxidant networks causing oxidative stress (Alothaid, 2022; Awan et al., 2023; Chukwuma et al., 2023; Tönnies and Trushina, 2017). These superfluous ROS trigger toxicological effects on the phospholipids, proteins, DNA, and RNA in neurons, mitochondrial function and dynamics, calcium homeostasis, receptor trafficking, cellular architecture, and energy homeostasis (Ege and Şelimen, 2021; Phanrang et al., 2022; Tönnies and Trushina, 2017). Also, the excess ROS orchestrates endogenous antioxidants in the brain (especially glutathione), which contributes to damage in the frontal cortex and hippocampus, increased amyloid-beta deposition, and hyperphosphorylated tau protein (Tönnies and Trushina, 2017). Remarkably, the high susceptibility of the brain to oxidative damage compared with other organs is because of its high oxygen demand, an abundance of unsaturated lipids in peroxidizable form, and redox-active metals (iron and copper) coupled with low enzymatic and non-enzymatic antioxidant content (Mattioli et al., 2020; Ogunro et al., 2022). Consequently, oxidative stress is at the fulcrum of the age-related spectrum of neurological diseases, not limited to amyotrophic lateral sclerosis, Parkinson's disease, Huntington's disease, and Alzheimer's disease (Capatina et al., 2020; Phanrang et al., 2022).

Alzheimer's disease (AD) is a major neurodegenerative damage characterized by behavioral disturbance, cognitive impairment, memory loss, communication problems, and a variety of neuropsychiatric symptoms (Dos Santos et al., 2018). International Alzheimer's Association reported in 2018 that about 50 million people globally have dementia caused mainly by AD, which is predicted to reach 152 million by 2050 (Ayaz et al., 2022). As such, AD has become a paramount public health concern and the fifth major causes of mortality among the aging population globally (Hampel et al., 2021). Although, studies have revealed that AD pathology is multifactorial, involving epigenetic, environmental, molecular and genetic factors (Ayaz et al., 2022). There are four proposed hypothesis implicated in pathophysiological process for the progression of AD ranging from the aggregation of Aβ peptide to form senile plaques (β-amyloid), excessive phosphorylation of tau to neurofibrillary tangles (tau protein), oxidative hypothesis, and loss of cholinergic neurotransmission (Ayaz et al., 2022; Ojo et al., 2021b). However, among the proposed hypothesis, the cholinergic model, which posits that a decline in two neurotransmitters, acetylcholine, and butyrylcholine, in the cerebrum triggers AD is the most widely studied. Neuropathological studies and clinical reports from the brain of dementia and AD patients have consistently shown damage or defect in the cholinergic pathways (Capatina et al., 2020). So, decline in acetylcholine and butyrylcholine have been closely associated with the early cognitive decline prevalent in AD patients (Dos Santos et al., 2018; Ojo et al., 2021b).

Over the years, several agents targeting the derangement in cholinergic dysfunction have been employed as a treatment regime for AD (Ayaz et al., 2022). It is intriguing to note that antagonists of acetylcholinesterase (AChE) and butyrylcholinesterase (BChE) inhibit the excessive breakdown of a neurotransmitter, acetylcholine, in the brain, thereby increasing their levels at the synaptic cleft, which enhances nerve cell communication and cognitive balance (Dos Santos et al., 2018). Currently, cholinesterase inhibitors: rivastigmine, donepezil, and galantamine approved for the treatment of AD only provide symptomatic relief transiently but cannot stop disease progression (Ojo et al., 2021b; Tönnies and Trushina, 2017). Unfortunately, their poor availability and low specificity trigger harmful impacts on the liver and other vital organs (Kpemissi et al., 2023). Several bedside-to-bench investigations are geared towards developing better pharmacotherapy of AD from natural sources to remedy this ugly situation. Besides, their safety profile, availability, accessibility, and additional therapeutic efficacy, particularly as antioxidants, will have a multi-targeted approach against AD onset and progression (Dos Santos et al., 2018).

Aframomum melegueta, also known as grain of paradise or alligator pepper, is a member of the Zingiberacea family (Ojo et al., 2021a). The reddish brown seed is used as a condiment in African and European cuisines (Ojo et al., 2021a). In the folk system of medicine, the seed decoration is used to treat toothache, fever, sore throat, hypotension, erectile dysfunction, and postpartum hemorrhage (Abdou et al., 2021). Among the pharmaceutical activities registered in the plant are anti-diabetic, anti-cancer, antioxidant, anti-hypotensive, and anti-inflammatory activities (Abdou et al., 2021; Ojo et al., 2021a). This study investigated the antioxidant and anti-cholinesterase inhibitory potential of crude and fractions of *Aframomum melegueta* seeds using a bioassay-guided approach. In addition, phytochemical characteriza-

tion of the most active fraction was carried out using a gas chromatography–flame ionization detector (GC-FID). Furthermore, chemoinformatics studies via molecular docking, MM/GBSA binding energy calculation, drug-likeness, and pharmacokinetic properties were conducted to investigate the therapeutic value of *A. melegueta* seeds phytochemicals as potent AD antagonists.

2. Materials and methods

2.1. Schematic overview of the experimental design

The schematic overview of the bioassay-guided experimental design is depicted in Fig. 1, demonstrating the major stages, from the extraction of the seeds with methanol to get the methanol extract to solvent–solvent fractionation with solvents of different polarity to obtain the n-hexane fraction, ethylacetate fraction,and aqueous methanol fraction. All the fractions and the crude extract were subjected to *in vitro* antioxidant tests using the following assays: Folin–Ciocalteau (TPC), and aluminium chloride reagents (TFC), 2,2-diphenyl-2-picrylhydrazyl (DPPH) radical scavenging activity, nitric oxide scavenging activity (NO), lipid peroxidation (TBARS) activity and ferric reducing power assay (FRAP). The two most active fractions (n-hexane and ethylacetate fractions), as revealed from their IC_{50} values, were further screened to investigate their AChE and BuChE inhibitory potentials. After that, phytochemical screening of the most potent fraction (ethylacetate fraction) was done using gas chromatography-flame ionization detector (GC-FID) analytical techniques, and the identified ligands were subjected to in silico studies, including molecular docking, MM/GBSA binding energy calculation, drug-likeness, pharmacokinetic and toxicity properties to determine the AD therapeutic lead compounds.

2.2. Chemicals, drugs, and reagents

The following analytical grade chemicals, drugs, and reagents used for the study were sourced as follows: acetylthiocholine iodide, aluminum chloride, ascorbic acid, butylated hydroxytoluene (BHT), butrylcholine iodide,chloroform, DTNB (5,5′-dithiobis-2-nitrobenzoic acid), Ellman's reagent, EDTA, ethanol, ferric chloride, gallic acid, Griess reagent, 1,1-diphenyl-2-picrylhydrazyl (DPPH), phospomolybdate, phosphotungstate, potassium acetate, potassium hexacyanoferrate (III), rutin, sodium phosphate buffer, sodium nitroprusside, andtrichloroacetic acid were sourced from Sigma Aldrich (St. Louis, MO, USA); ethyl acetate, n-hexane, methanol, sodium trioxocarbonate (IV), pyridine, thiobarbituric acid (TBA), were products of British Drug House (Poole, England) while rivastigmine was gotten from reputable pharmacy shop. All the reagents and chemicals were prepared freshly using distilled water.

2.3. Plant preparation, extraction, and partitioning

The dry pods of *A. melegueta* was purchased and the seeds were pulverized with a mechanical blender to get 243.8 g powder, and extracted through cold maceration in 2 L of absolute methanol for 72 hrs. Filtration was done firstly with muslin cloth followed by Whatman filter paper no 1 with a pore size of 11 m. Next, the filtrate was concentrated under reduced pressure at 45 °C using a rotatory vacuum evaporator (R-215, Buchi, Flawil, Switzerland) to obtain the methanol extract of *A. melegueta* (MEAM). Then, MEAM was subjected to solvent–solvent partitioning using n-hexane, ethyl acetate, and water to get the n-hexane, ethyl acetate, and the aqueous-methanol fractions of *A. melegueta* designated as HFAM, EFAM, and AMFAM, respectively. Finally, all the fractions obtained were concentrated in a rotary evaporator and stored in the refrigerator till when needed.

2.4. Determination of total phenol content (TPC)

Total phenolic contents of the methanol extract and fractions of *A. melegueta* were investigated with Folin–Ciocalteau's reagent following Singleton and Rossi, (1965) method. Folin–Ciocalteau's reagent was freshly prepared with phospomolybdate and phosphotungstate. An aliquot, 0.5 mL of the Folin-ciocalteau reagent (1/10 dilution), and Na_2CO_3 2% (1.5 mL w/v) were added to 0.5 mL of the methanol extract and fractions of *A. meleguata*. Finally, the resulting mixture was incubated for 15 min at 45 °C, and absorbance was measured at 765 nm using a spectrophotometer. Thereafter, TPC expressed as milligrams of gallic acid equivalent (GAE) per gram of sample was calculated using a gallic acid standard curve.

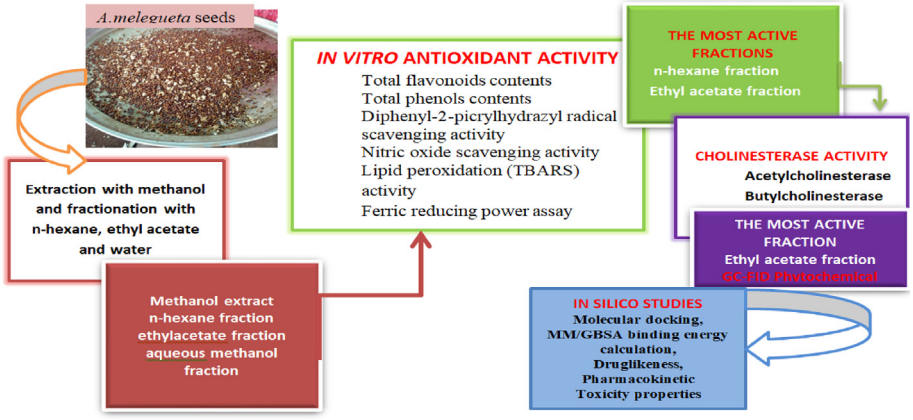

Fig. 1 Schematic diagram of the bioassay guided experimental design.

2.5. Determination of total flavonoid contents (TFC)

The total flavonoids contents of the extract and fractions expressed as rutin equivalent in mg/g were determined using aluminum chloride in a colorimetric method according to Zhishen et al., (1999) standard protocol. An aliquot, 1 mL each of the extract and fractions were pipetted to a test tube containing 0.2 mL of aluminum chloride prepared in methanol (10% (w/v)), 0.2 mL of 1 M potassium acetate and distilled water (5.6 mL). The mixture was vigorously shaken and incubated at room temperature for 30 min and the absorbance read at 415 nm. The analysis was performed in triplicate, and the TFC was calculated from the rutin calibration curve generated.

2.6. In vitro steady-state antioxidant activity

2.6.1. 2,2-Diphenyl-1-picrylhydrazyl (DPPH) radical-scavenging assay

The ability of the crude methanolic extract and fractions of *A. melegueta* to stabilize DPPH free radicals was investigated using Gyamfi et al., (1999) experimental protocols. To 1 mL of varying concentration (15.63–500 µg/mL) of the extract and fractions in methanol and ascorbic acid (standard antioxidant) were added 0.5 mL of 0.076 mm DPPH solution in methanol. The mixture was shaken and incubated for 25 min in the dark at room temperature. Subsequently, the solution's absorbance was measured against a blank at 517 nm. Inhibition of DPPH (%) of the three replicate values of each sample was calculated as shown below using Eq. (1):

$$\text{Inhibition of DPPH } (\%) = \frac{Abs\ control - Abs\ sample}{Abs\ control} \times 100 \quad (1)$$

where Abs = Absorbance.

2.6.2. Nitric oxide scavenging activity

The scavenging activity of the extract and fractions against nitric oxide generated *in vitro* from sodium nitroprusside was evaluated according to the method of Sreejayan and Rao, (1997). A volume, 3 mL of sodium nitroprusside (10 mmol/L) in phosphate buffer saline (0.2 mmol/L, pH 7.4) was added to test tubes containing various concentrations (15.63–500 µg/ml) of the extract/fractions. Subsequently, the test tubes were incubated at 25 °C for 150 min, and then 500 µL of Griess reagent (1% sulphanilamide, 2% orthophosphoric, 0.1% N-napthylethenediamine dihydrochloride) was added. The absorbance was finally measured spectrophotometrically at 546 nm. The protocol was also done with ascorbic acid used as the standard. Nitric oxide (NO) inhibitory properties of the three replicate values of each sample were calculated with the Eq. (2) below:

$$\text{Inhibition of NO } (\%) = \frac{Abs\ control - Abs\ sample}{Abs\ control} \times 100 \quad (2)$$

where Abs = Absorbance.

2.6.3. Lipid peroxidation (TBARS) assay

The extent of inhibition of lipid peroxidation by the extract and fractions was determined by measuring thiobarbituric acid-reactive substances (TBARS) using a standard protocol of Banerjee et al., (2005). First, an aliquot, 100 µL of the extract and fractions prepared in graded concentrations (15.63–500 µg/mL), and 500 µg/mL of egg yolk homogenate (lipid-rich media) were mixed, and the volume made up to 1.0 mL with distilled water. This was followed by adding $FeSO_4$ (50 µL of 0.075 M) and L-ascorbic acid (20 µL) and incubating at 37 °C at room temperature for 1 hr. Then, 15 mL of TBA reagent and 0.2 mL of EDTA (0.1 M) were added, and each sample was cooked for 15 min at 100 °C. Thereafter, the cooked samples were centrifuged for 10 min, and absorbance was taken at 532 nm. Butylated hydroxytoluene (BHT) served as the standard drug. Inhibition of lipid peroxidation was calculated using equation3:

$$\text{Inhibition of lipid peroxidation } (\%) = \frac{Abs\ control - Abs\ sample}{Abs\ control} \times 100 \quad (3)$$

where Abs = Absorbance.

2.6.4. Ferric reducing antioxidant power assay (FRAP)

The power of the extract and fractions of *A. melegueta* to reduce ferric ions was investigated using the experimental procedure of Oyaizu, (1986). One milliliter of the extract and fractions at various concentrations (15.63–500 µg/mL) were incubated for 20 min at 50 °C in sodium phosphate buffer (0.2 M) containing potassium hexacyanoferrate (III) (1%). Then, 2 mL of trichloroacetic acid (10%) was added, and the mixture was centrifuged. The supernatant was mixed with ferric chloride (0.1%), and the solution's absorbance was measured at 700 nm. The percentage FRAP activity of the three replicate values was calculated and reported in Gallic acid equivalent (GAE).

2.7. Cholinesterase inhibitory assay

The acetylcholinesterase and butyrylcholinesterase inhibitory effects of n-hexane and ethylacetate fractions of *A. melegueta* were assayed following the experimental procedure of (Ellman et al., (1961). Rivastigmine was the standard drug used, while the substrates were acetylcholine iodide (ATChI) and butyrylcholine iodide (BTChI), respectively. Concisely, 20 µL each of varying concentrations (15.63–500 µg/mL) of the fractions and rivastigmine in methanol were carefully pipetted into the microplates before adding 240 µL of phosphate buffer with pH 8.0, and 20 µL of the enzymes. The plates were vortexed and incubated for 30 min at 37 °C. Subsequently, 20 µL of 25 mM of the substrates (ATChI and BTChI) and 20 µL of 5, 50 -Dithiobis-2-nitrobenzoic acid (10 mM) were added to the reaction media. Enzymatic hydrolysis of the substrates was assayed spectrophotometrically at 412 nm with methanol as the negative control. The experiment was conducted in triplicate. The enzymes (AChE and BuChE) inhibitory activities of the fractions were calculated as follows with Eq. (4):

$$\text{Cholinesterase inhibition } (\%) = \frac{Abs\ control - Abs\ sample}{Abs\ control} \times 100 \quad (4)$$

where Abs denotes absorbance.

2.8. Phytochemical screening of ethylacetate fraction of A. melegueta using gas chromatography–flame ionization detector (GC-FID)

Preparation of the fraction, screening, and identification of the phytochemicals present in the ethylacetate fraction of *A. melegueta* was done following the experimental protocol reported in our previous studies Chukwuma et al. (2022) using BUCK M910 gas chromatography coupled to a flame ionization detector. In quantitative analysis, 150 µL of betulin solution was added to each vial before derivatization. Thereafter, the analysis was carried out on a RESTEK 15-m MXT-1 column with dimensions 15 m × 250 µm × 0.15 µm. The sample (2 µL) was injected into the column heated at a temperature of 280 °C and with 30 cm/slinear velocity. The carrier gas used was Helium 5 PSI with a 40 Ml/min flow rate. Initially, the oven was operated at 200 °C, after which the temperature was increased at a rate of 3 °C/min to 330 °C, and the column temperature was maintained for 5 min. Subsequently, the detector operating temperature was adjusted to 320 °C. Quantification of the phytochemicals present in the eluted sample was done by calculating the ratio between the area and mass of internal standard and the area of the identified phytochemicals. Finally, concentrations of the different phytochemicals identified in the fraction were expressed in µg/g. 2D structures of the identified compounds were retrieved from ChemDB Chemoinformatics portal (https://chemdb.ics.uci.edu/cgibin/Smi2DepictWeb.py).

2.9. Chemoinformatics studies

2.9.1. Retrieval and preparation of crystal protein structure

The x-ray crystallography structure of acetylcholinesterase (AChE) and butyrylcholinesterase (BChE) was retrieved from the Protein Data Bank (PDB) using the identifiers 4EY7 and 1P0M, respectively. The crystallized structure was co-crystallized with donepezil in its catalytic active site, whereas BChE had choline as a co-crystallized ligand. The qualities of the structures and reasonable solution (below 2.5 Å) informed our decision to choose this structure (Tysoe et al., 2019). The protein preparation wizard (PPW) of Schrodinger suite v12.4 was used to prepare the retrieved PDB structure for molecular docking studies. The PPW assigned bond orders, added missing hydrogens, simulated missing disulfide bonds, converted selenomethionine to methionine, filled up missing side chains and loops, removed waters molecules beyond 5 Angstrom, and finally minimized the restrained energy of the structure. The quality of the preprocessed structure was assessed by the protein reliability report and Ramachandran plot (Supplementary Fig. 1).

2.9.2. Preparation of Ligand's library

The phytochemicals identified by the GC-FID analysis from the ethyl acetate fraction was used to build library of compounds for this study. The canonical SMILES representation of the screened phytochemicals was retrieved from PubChem (https://pubchem.ncbi.nlm.nih.gov/), and their optimal, energy-minimized 3D conformation was generated using the LigPrep tools of the Schrodinger suite v12.03. Rivastigmine (PubChem ID: 77991) was adopted as the standard drug, and its structure (3D) was added to the ligand library.

2.9.3. Binding site predictions and grid generation for molecular docking

The binding pockets/catalytic active sites of both enzymes (AChE and BChE) were predicted with Schrodinger suite v12.03 advanced sitemap tools. The software annotated and scored binding pockets of high likely hood to bind/accommodate small molecules based on their volumes, the nature of their amino acid residues, and another favorable physiochemical parameter. The best binding site (Site_1 and Site_2) for the two enzymes, AChE and BChE, respectively, was selected based on the site score, D score, and volume (Supplementary Tables 1 and 2). Furthermore, Grid Generation tools of Schrodinger suite was used to generate the docking grid (as represented in Supplementary Fig. 2 was generated around the most probable binding site). The Grid ensured site-directed docking of the ligands (phytochemicals of ethylacetate fraction of *A. melegueta*) and standard (Rivastigmine) to the most probable binding/catalytic site.

2.9.4. Molecular docking experiments

Molecular docking of the compounds (phytoligands) and standard was conducted using the SP-GLIDE (Standard precision) and XP-GLIDE (extra-precision) docking models, the phytochemical libraries were docked at the most probable binding site of AChE and BChE. In addition, the interaction for hit compounds (selected based on the X-glide score) was further examined for their 2D and 3D interaction.

2.9.5. In silico validation of the docking program

The validation of the docking program was performed to estimate the reliability of the docking experiment. First, we investigated the software's accuracy in predicting and annotate the binding site to which the co-crystallized ligands were bound in the apo-proteins as the top-ranked binding pocket. The corrected software predicted the binding pocket where the co-crystallized ligand was bound to as the best binding site for AChE and BChE (supplementary Tables 1 and 2). Secondly, we docked the co-crystallized ligand of AChE (donepezil) to the apo-protein structure of acetylcholinesterase (4EY7) and calculated the root mean square deviation (RMSD) of donepezil in the docked pose to the crystal structure pose (Supplementary Fig. 3). The obtained root mean square deviation (RMSD) was 0.6122 Å between the docked pose and the crystal structure pose, inferring the excellent reliability of the docking software. According to El-Kelawy et al. (2017) an RMSD below 2 Å is excellent for docking.

2.9.6. Binding free energy calculation

The binding free energy (ΔG_{bind}) of the hits compounds to the crystallized protein AChE (4EY7) and BuChE (1P0M) was calculated using the molecular mechanics generalized Born

surface area (MM-GBSA) model of the Prime Package of Schrodinger v12.4. The OPLS3 force field and VSGB solvation model were adopted for the ΔG_{bind} calculation. The MM-GBSA model estimated the ΔG_{bind} according to the following equation.

$$\Delta G\text{bind} = \Delta E + \Delta G_{solv} + \Delta G_{SA} \quad (5)$$

$$\Delta E = E_{complex} - E_{protein} - E_{ligand} \quad (6)$$

where $E_{complex}$, $E_{protein}$, and E_{ligand} are the minimized energies of the protein–inhibitor complex, protein, and inhibitor, respectively.

$$\Delta G_{solv} = G_{solv(complex)} - G_{solv(protein)} - G_{solv(ligand)} \quad (7)$$

where $G_{solv(complex)}$, $G_{solv(protein)}$, and $G_{solv(ligand)}$ are the salvation-free energies of the complex, protein, and inhibitor, respectively.

where

$$DG_{SA} = G_{SA(complex)} - G_{SA(protein)} - G_{SA(ligand)} \quad (8)$$

are the surface area energies for the complex, protein, and inhibitor, respectively.

2.9.7. ADMET prediction

The hit compounds' Adsorption, Distribution, Metabolism, and Excretion (ADME) profile were predicted using the SwissADME web server (https://www.swissadme.ch/,). Prediction of toxicity and toxicological effects of the identified compounds was done with ProTox-II webserver (ProTox-II - Prediction of TOXicity of chemicals, https://tox-new.charite.de/protox_II). The ProTox-II web server incorporates molecular similarity, pharmacophores, fragment propensities, and machine-learning models to predict oral toxicity, organ toxicity (hepatotoxicity), and toxicity endpoints (carcinogenicity, immunogenicity, mutagenicity, and cytogenecity).

2.10. Statistical analysis

The triplicate data sets generated were descriptively analyzed with one-way analysis of variance (ANOVA) using $p < 0.05$ as the least significant threshold. Duncan and turkey's post hoc multiple comparisons were also performed with the help of the IBM statistical package for windows version 23 (SPSS Inc., Chicago, IL, USA). The half maximal inhibitory concentration (IC_{50}) and Goodness of Fit (R square) of the datasets were obtained from the concentration versus inhibition nonlinear regression curves thanks to GraphPad Prism version 6.05 (GraphPad Software, Inc., California, USA).

3. Results

3.1. Total phenols and flavonoids contents of the extract and fractions of *A. melegueta* seeds

The total phenols (TPC) content expressed in GAE show that both extract and fractions of *A. melegueta* had remarkably high phenolic content, ranging from 483.6 to 633.13 mg GAE/g. The Ethylacetate fraction had the highest TPC (633. 13 ± 5.62 mg GAE/g), followed by the methanol extract (607 ± 6.95 mg GAE/g) and aqueous-methanol fraction (523.79 ± 16.14 mg GAE/g), while the lowest TPC was found in n-hexane fraction (483.6 ± 10.40 mgGAE/g). Similarly, the total flavonoids contents (TFC) of ethylacetate fraction (711. 04 ± 15.24 mgRT/g) was highest, followed by crude methanol extract (209.17 ± 12. 70 mg RT/g) and aqueous methanol fraction (195.21 ± 13.21 mg RT/g), the lowest total flavonoids were seen in the n-hexane fraction (66.25 ± 8.86) (Table 1).

Results are reported as mean ± SD of triplicate determination at a 95% confidence interval. Significant difference denoted by different alphabets at $p < 0.05$ was obtained with one-way ANOVA followed by LSD and Duncan post hoc multiple comparisons.

3.2. In vitro antioxidants activity

3.2.1. DPPH radical scavenging activity of extract and fractions of A. melegueta seeds

The extract/fractions had high DPPH radical scavenging activity, which was highest at 500 µg/mL, where radical scavenging activities of 83.08 ± 2.75, 83.25 ± 1.64, 85.40 ± 0.87, and 76.22 ± 7.13 in percentages were found in methanol extract, n-hexane, ethylacetate and aqueous- methanol fractions respectively (Fig. 2A). Overall, among the extract and fractions, EFAM showed the highest (IC_{50} value 5.06 and R^2 0.9547) activity, followed by HFAM (IC_{50} value 5.08 and R^2 0.9389), and AMFAM (IC_{50} value5.43 and R^2 0.9342) and the least being the MEAM which had estimated IC_{50} value of 5.62 and R^2 0.9476. Interestingly, the DPPH radical scavenging activity of the extract and fraction were found to be relatively higher than that of the standard antioxidant, ascorbic acid (IC_{50} value9.526.886 µg/mL and R^2 0.9943) (Table 2).

3.2.2. NO scavenging activity of extract and fractions of A. melegueta seeds

The results in Fig. 2B and Table 2 show that the extract/fractions had good nitric oxide inhibitory effects. EFAM depicted the highest NO scavenging activity with an IC_{50} value of 6.58 µg/ml against 7.40, 7.75, and 9.01 µg/mL recorded for AMFAM, HFAM, and MEAM, respectively. The NO inhibi-

Table 1 Total phenols and flavonoids contents of the extract and fractions of *A. melegueta* seeds.

Extract/fractions	Total Phenols contents(mg GAE/g)	Total Flavonoids contents(mg RT/g)
Methanol extract	607.53 ± 6.95[b]	209.17 ± 12.70[b]
Ethylacetate fraction	633.13 ± 5.62[b]	711.04 ± 15.24[c]
n-Hexane fraction	483.6 ± 10.40[a]	66.25 ± 8.86 [a]
Aq-methanol fraction	523.79 ± 16.14[a]	195.21 ± 13.21[b]

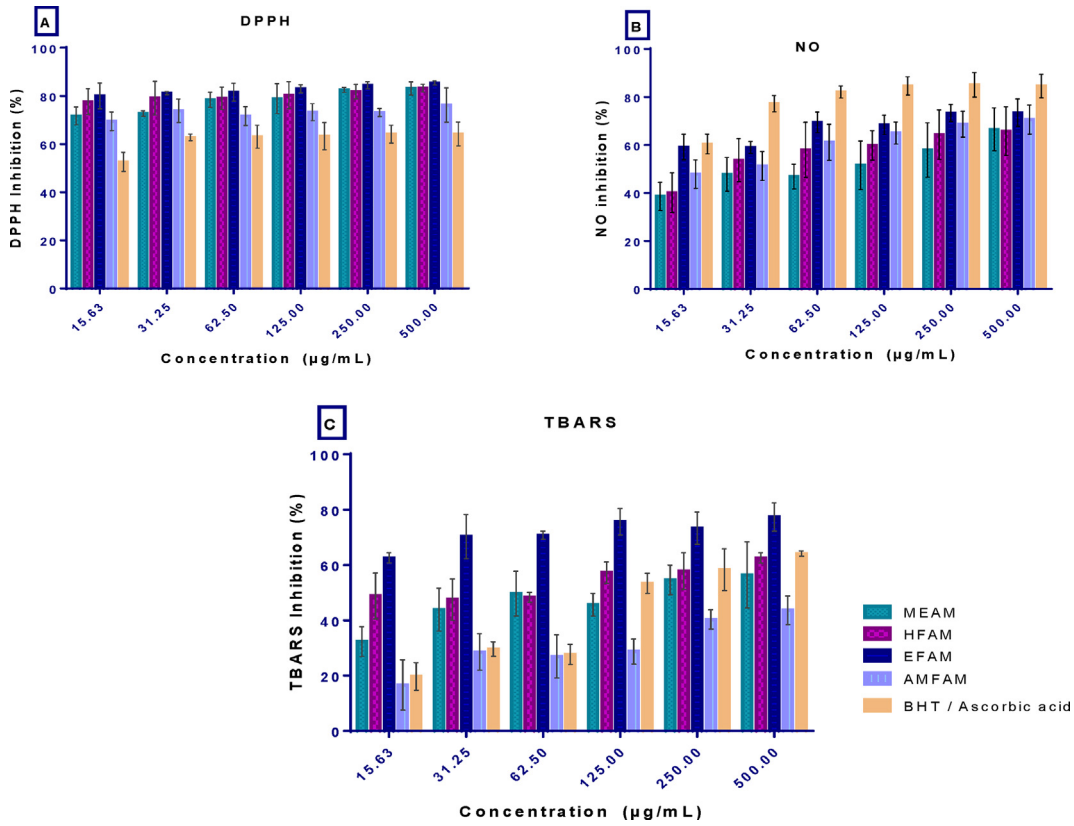

Fig. 2 In vitro antioxidant activity of the extract and fractions of A. melegueta seeds and standards (A) 2,2-diphenyl-2-picrylhydrazyl (DPPH) radical scavenging activity, (B) nitric oxide scavenging activity (NO) and (C) lipid peroxidation (TBARS) activity. Results are reported as mean ± SD of triplicate determination.

Table 2 Half maximal inhibitory concentrations (IC_{50}) of all the antioxidant assays.

IC_{50} values (µg/mL)						
Assays	**MEAM**	**HFAM**	**EFAM**	**AMFAM**	**AA**	**BHT**
DPPH scavenging	5.62	5.08	5.06	5.43	6.886	–
NO scavenging	9.00	7.75	6.58	7.40	4.667	–
TBARS inhibition	8.73	3.44	2.12	25.79	–	18.14
Ferric reducing	107.10	99.12	88.73	117.6	–	–
Overall IC_{50} values	130.45	115.39	102.49	156.22		

tory effect of the EFAM, AMFAM, HFAM, and MEAM was positively correlated with concentration, having R_2 values of 0.6255, 0.7447, 0.7466, and 0.6106, respectively. However, the standard drug, ascorbic acid, demonstrated higher NO scavenging activity and hence lower IC_{50} 4.667 and R^2 0.9622.

3.2.3. Lipid peroxidation inhibitory effect of extract and fractions of A. melegueta seeds

The results of the thiobarbituric acid scavenging activity in Fig. 2C show that the extract, fractions, and standard drug, Butylated hydroxytoluene (BHT), had maximal TBARS inhibition at 500 µg/ml. EFAM was the most potent TBARS inhibitor, followed by HFAM and MEAM, while the least inhibition was recorded in AMFAM, as revealed from their IC_{50} values of 2.12, 3.44, 8.73, and 25.79, respectively. Taken together, the EFAM, HFAM, and MEAM demonstrated better TBARS inhibitory effects than BHT which had an IC_{50} value of 18.14 (Table 2).

3.2.4. Ferric reducing antioxidant power

As presented in Fig. 3, the FRAP inhibitory capacity expressed in GAE shows a non-concentration dependent activity which was optimal at 15. 63 µg/mL with values of 5.33 ± 0.20, 4.06 ± 0.79, 3.83 ± 0.13, and 2.78 ± 1.075GAE, recorded for HFAM, AMFAM, EFAM, and MEAM, respectively, against 0.25 ± 0.02, 0.19 ± 0.01, 0.37 ± 0.33, and 0.11 ± 0.02 obtained at 500 µg/mL, respectively. From the regression curve, the EFAM had the highest reducing power

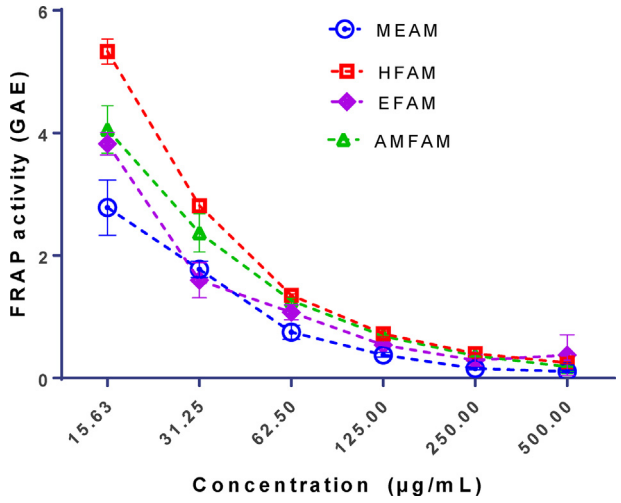

Fig. 3 Ferric Reducing Antioxidant Power of the extract and fractions of *A. melegueta* seeds. Results are reported as mean ± SD of triplicate determination.

with an IC_{50} value of 88.73 µg/mL, followed by HFAM (IC_{50} 99.12 µg/mL), MEAM (IC_{50} 107. 10 µg/mL), and AMFAM (IC_{50} 117.60 µg/mL) (Table 2).

3.2.5. Half maximal inhibitory concentrations (IC_{50}) of the extract and fractions in all the antioxidant assays

Results in Table 2, which represents the overall IC_{50} values of the extract and fractions in all the, revealed that EFAM (IC_{50} values102.49 µg/mL) had the highest antioxidant inhibitory potential, followed by the HFAM (IC_{50} values 115.39 µg/mL), MEAM (IC_{50} values 130.45 µg/mL). In contrast, the least inhibitory effect was estimated in the AMFAM (IC_{50} values 156.22). The higher antioxidant effect of HFAM and EFAM formed the basis for the evaluation of their cholinesterase inhibitory efficacy.

3.3. Cholinesterase activity

3.3.1. Acetylcholinesterase (ACHE) inhibitory activity of n-hexane and ethyl acetate fractions of A. melegueta seeds

The results of the AChE inhibitory potential of HFAM and EFAM revealed that both fractions inhibited the enzyme activity in a concentration-dependent manner, just like the reference drug, rivastigmine. Thus, maximal enzyme inhibitory activity of 82.74 ± 3.21, 85.88 ± 5.21, and 83.34 ± 4.66 was recorded for HFAM, EFAM, and rivastigmine, respectively at 500 µg/mL. Comparatively, the AChE activity inhibitory effect demonstrated by EFAM IC_{50} 11.67 µg/mL and R^2 0.9898 was similar to that of rivastigmine (IC_{50} 11.99 µg/mL and R^2 0.9981) but higher than that of HFAM (IC_{50} 16.83 µg/mL and R^2 0.9556) (Fig. 4).

3.3.2. Butyrylcholinesterase (BuChE) inhibitory activity of n-hexane and ethylacetate fractions of A. melegueta seeds

In this study, EFAM and HFAM also inhibited BuChE in a concentration-dependent manner. However, the inhibitory activity of EFAM with IC_{50} value of 5.21 µg/mL and R^2 0.9683 was higher than that of HFAM with IC_{50} 16.64 µg/mL and R^2 0.9939. Interestingly, both fractions were found

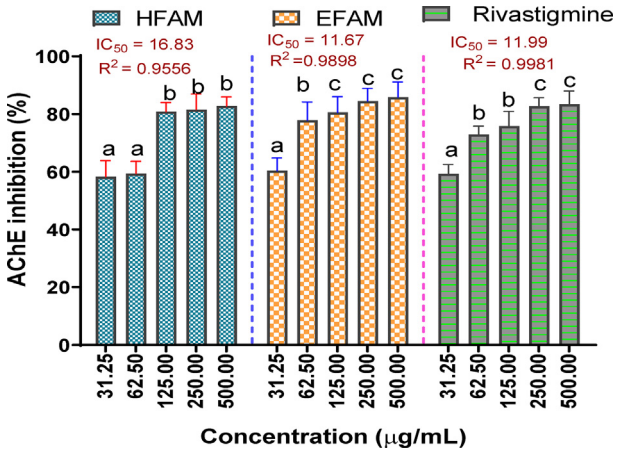

Fig. 4 Acetylcholinesterase inhibitory activity of n-hexane and ethyl acetate fractions of *A. melegueta* seeds**.** Results are reported as mean ± SD of triplicate determination. Percentage inhibition of a sample across varying concentrations (31.25–500 µg/mL) with a different alphabet are statistically significant at $p < 0.05$. However, values with the same lettered alphabet are not significantly different ($p < 0.05$).

to be more potent inhibitors of BuChE than rivastigmine (IC_{50} value of 11.40 µg/mL and R^2 0.9816) (Fig. 5).

3.4. GC-FID phytochemical profiling of ethyl acetate fraction of A. melegueta seeds

The GC-FID proofing of the EFAM revealed that the ethylacetate fraction is kaempferol (40.0045 µg/g) enriched. EFAM

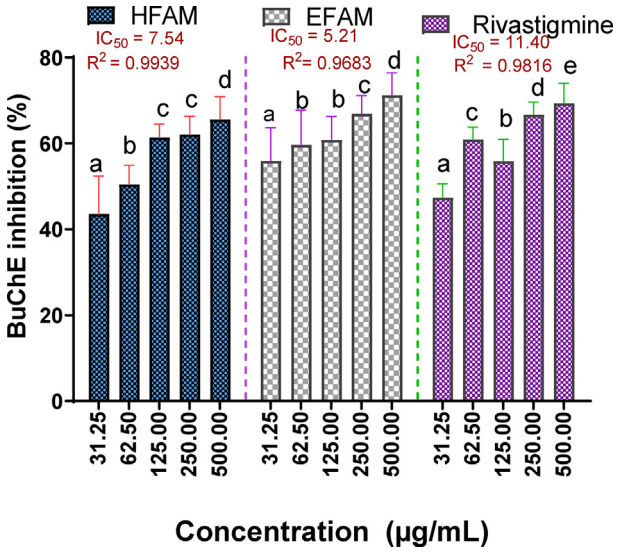

Fig. 5 Butyrylcholinesterase inhibitory activity of n-hexane and ethyl acetate fractions of *A. melegueta* seeds. Results are reported as mean ± SD of triplicate determination. Percentage inhibition of a sample across varying concentrations (31.25–500 µg/mL) with a different alphabet are statistically significant at $p < 0.05$. However, values with the same lettered alphabet are not significantly different ($p < 0.05$).

also contains an abundance of cyanogenic glycosides (19.9918 ppm), tannin (8.3918 ppm), ammodendrine (7.9895), and ribalinidine (7.2622 ppm), while the least occurring phytochemicals in decreasing order were anthocyanin (3.6623 ppm) > naringenin (2.3219 ppm) > aphylidine (2.0001 ppm) > oxalate (0.6294 ppm) and dihydrocytisine (0.3903 ppm) (Fig. 6 and Table 3). The compounds contain bioactive functional groups, as shown in Fig. 7.

3.5. Chemoinformatics

3.5.1. Quality of the preprocessed crystal protein structure and ligands

The Ramachandran plots of the processed crystal structures of the protein (Supplementary Fig. 1a and b), as well as the protein reliability report, showed the relative suitability of the selected x-ray crystal structure of AChE (4EY7) and BuChE (1P0M), used for the molecular docking experiment. The prepared structure was of good quality as there were no Ramachandran outliers, but only a few glycine and proline residues represented as triangle and rectangle dots, respectively (which do not significantly affect the overall suitability of the structures). The prepared protein structure had excellent protein packing and no missing loops, bond angle deviation, and unusual B-factor.

3.5.2. Molecular docking

Based on the docking score and ligand efficiencies, the best-scoring compounds that had good docking scores with both AChE and BuChE were shown in Table 4. Catechin, and kaempferol interacted with AChE with docking scores of −10.78, and −9.22, respectively, where their interaction with BuChE gave docking scores of −10.29 and −9.813 kcal/mol, respectively which was better than −7.45 and −7.499, respectively recorded in the standard, rivastigmine (Table 4). Their interactions within the enzymes amino acid residues were analyzed and presented in Table 4, while the 3D and 2D structures are in Figs. 8 (AChE) and 9 (BuChE).

3.5.3. Validation of the docking program

The docking program validation was performed to check the software's reliability for molecular docking. In this study, the co-crystalized ligand (donepezil) was docked onto the apo-acetylcholinesterase protein (AChE – 4EY7), and the root mean square deviation (RMSD) of the docked pose and the crystal structure pose of the co-crystallized (donepezil) after superimposition was calculated (Supplementary Fig. 2). The docking program was excellent for the study as the root mean square deviation (RMSD) was 0.6122 Å between the docked pose and the crystal structure pose. An RMSD below 2 Å is excellent for docking (El-Kelawy et al., 2017).

3.5.4. Binding free energy calculation using the prime MM-GBSA model

The binding energy calculation for the best pose of the extra-precision molecular docked complex was calculated for the hits – Catechin, and kaempferol, and the standard drug rivastigmine. Results from the calculation showed that all the hit compounds had above 35.0 kcal/mol (Table 5).

3.5.5. ADMET properties

Taken together, all the screened phytochemicals had zero Lipinski and Veber violations, bioavailability score of 0.55, high gastrointestinal absorption and non-inhibitors of CYP450 isoform CYP450 2C19 and 2C9. Acute toxicity prediction outcome showed that they have no tendency for hepatotoxicity, carcinogenicity, immunogenicity, mutagenicity, or cytotoxicity (Table 6).

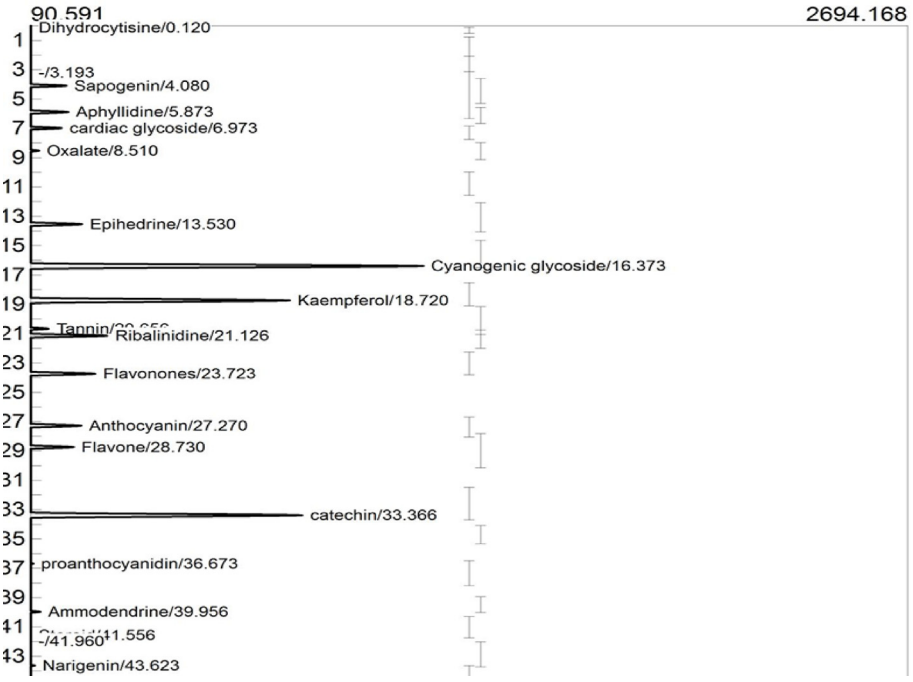

Fig. 6 GC-FID chromatogram of Phytochemical identified in ethyl acetate fraction of *A. melegueta* seeds.

Table 3 Phytochemicals identified in ethylacetate fraction of *A. melegueta* seeds using GC-FID.

Peaks	Identified Compounds	Retention time (min)	Peak Area	Peak height	Conc. (μg/g)	Class of compounds
1.	Dihydrocytisine	0.120	576.7934	62.913	0.3903	Alkaloid
2.	Sapogenin	4.080	2498.5069	195.448	3.9987	Saponin
3.	Aphyllidine	5.873	2552.6972	200.287	2.001	Alkaloid
4.	Cardiac glycoside	6.973	2304.8660	181.239	6.3613	Glycoside
5.	Oxalate	8.510	1449.3234	114.104	0.6294	Anti-nutrient
6.	Ephedrine	13.530	3073.7339	241.808	5.000	Alkaloid
7.	Cyanogenic glycoside	16.373	16362.1141	1254.769	19.9918	Glycoside
8.	Kaempferol	18.720	11013.1668	859.243	40.0045	Flavonoid
9.	Tannin	20.656	1806.6874	142.398	8.3918	Polyphenol
10.	Ribalinidine	21.126	4054.1099	317.498	7.2622	Alkaloid
11.	Flavonones	23.723	3584.5839	281.274	3.9999	Flavonoid
12.	Anthocyanin	27.270	3041.5790	239.335	3.6623	Flavonoid
13.	Flavone	28.730	2749.7988	216.419	4.9280	Flavonoid
14.	Catechin	33.366	11487.1835	895.989	3.9964	Flavonoid
15.	Proanthocyanidin	36.673	1303.6000	97.906	4.2315	Flavonoid
16.	Ammodendrine	39.956	1503.7382	118.164	7.9895	Alkaloid
17.	Naringenin	43.623	1295.6357	101.788	2.3219	Flavonoid
18.	Phytate	44.703	754.0485	59.230	5.0080	Anti-nutrient

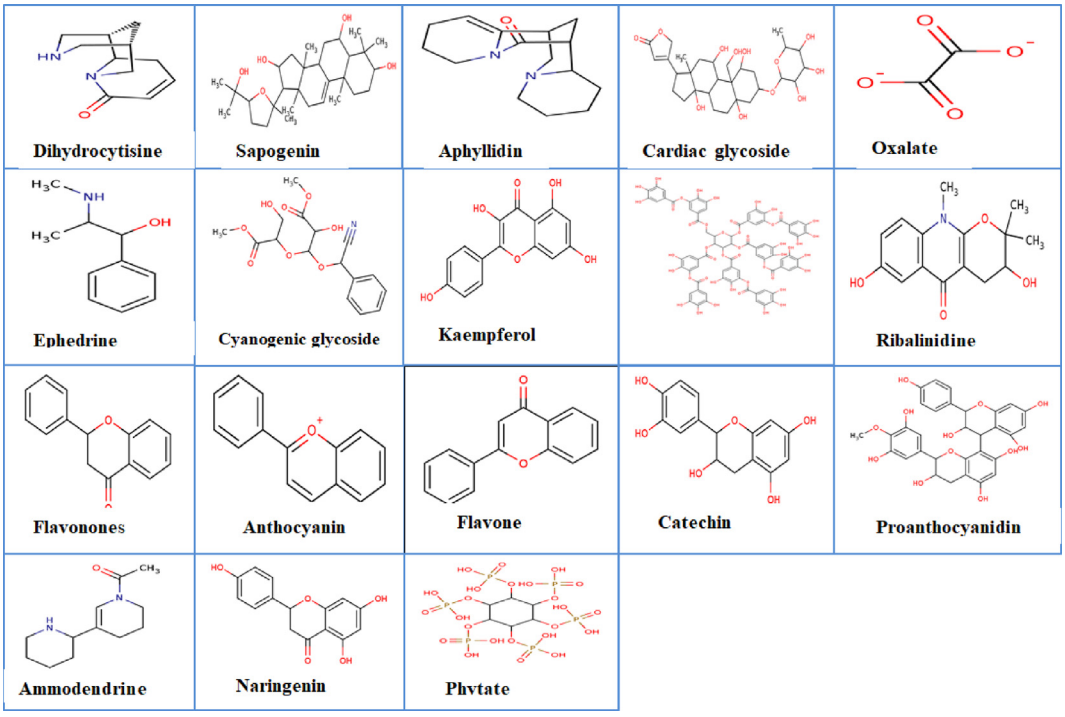

Fig. 7 2D structures of the phytochemicals present in ethylacetate fraction of *A. melegueta* seeds.

4. Discussion

Over the decade, several phytochemicals with biological and pharmaceutical actions are currently used as therapeutic agents for several diseases (Chukwuma et al., 2023; Nkwocha et al., 2022). Among the milieu of these phytochemicals are phenols and flavonoids. In this study, high abundance of TPC and TFC were registered in the extract and fractions of *A. melegueta*. The biochemical mechanisms of actions of phenolic compounds span from scavenging of free radicals and oxidants species, chelation of metal ions, decomposing of peroxides, regulation and stimulation of signaling pathways including transcription factor Nrf2 needed to protect cells against oxidative damage to regulation of cellular mediators (Chukwuma et al., 2020). Hence, it is intriguing to note that phenols terminate free-radical chain reactions, thereby preventing the onset of neurological diseases like AD (Elufioye et al., 2019). According to Silva and Pogačnik, (2020), dietary intake of phenolic compounds or their use as pharmacological drugs, nutraceuticals, or supplements is promising in prevent-

Table 4 Top selected compounds from the phytochemical library and their molecular docking scores obtained when XP-docked to AChE and BuChE.

Compounds	Docking scores (kcal/mol)	Interaction with amino acids
Acetylcholinesterase		
Catechin	−10.78	[h]PHE295,[h]TYR124,[h]GLY122,[h]SER203,[#]HIS447, [#]TYR341
Kaempferol	−9.215	[h]GLY122, [#]HIS447, [#]PHE338
Rivastigmine_(standard)	−7.45	[h]TYR124, *TRP286
Co-crystallized ligand	−16.969	[H]PHE295,*TYR337, *TRP86, [#]TRP86, [#]TRP286
Butyrylcholinesterase		
Catechin	−10.29	[h]ALA328, [h]THR120
Kaempferol	−9.813	[h]GLY115,[h]TYR128,[h]GIH197,[h]ALA328,[#]TRP82
Rivastigmine_(standard)	−8.449	*TYR332, [#]TRP82
Co-crystallized ligand	−4.004	*TRP82

[h]H-bond, *Pi-cation, [#]pi-pi stacking.

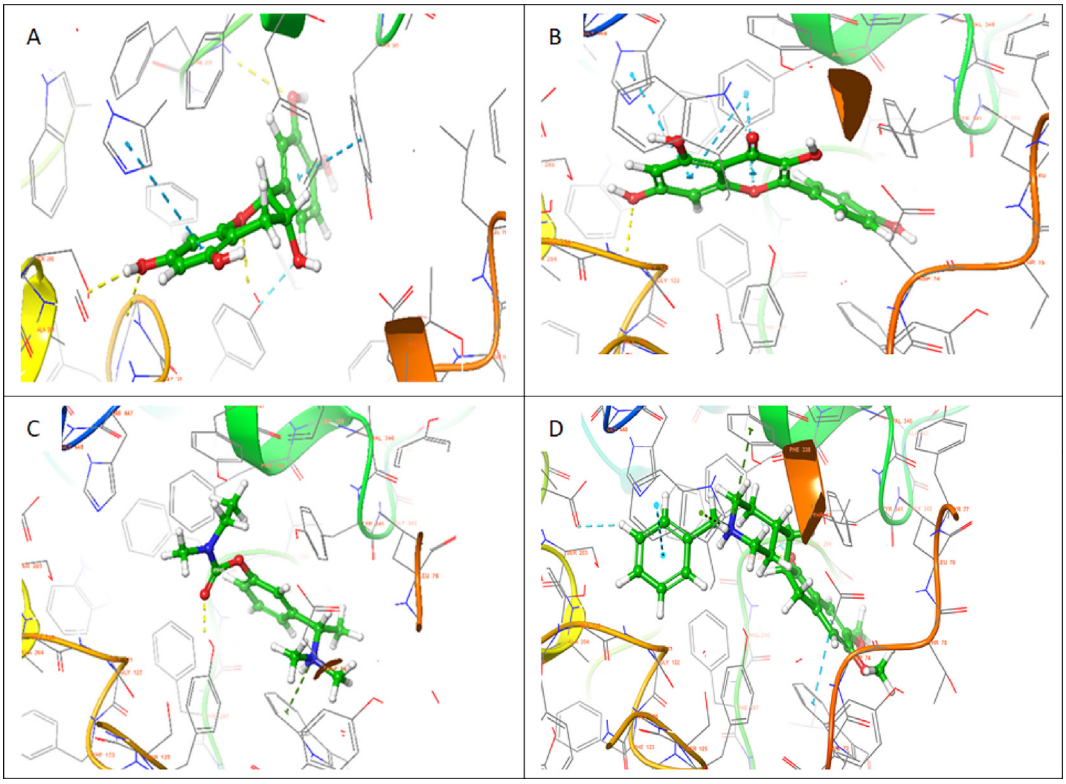

Fig. 8A 3D representation of molecular docking poses of selected compounds (A) catechin (B), kaempferol (C) Standard drug-Rivastigmine (D) Co-crystallized ligand in the binding pocket of acetylcholinesterase (4EY7).

ing neurodegenerative diseases. Also, regular consumption of flavonoids-rich foods can effectively restore cognitive capabilities in human, and prevent the progression of AD (Ayaz et al., 2019). Enhancement of neuronal function, protection against neuroinflammation, enhancement of blood flow to the brain and initiation of neurogenesis in the brain part involved in cognition are the mechanistic pathways of neuro-protective actions of flavonoids (Kent et al., 2017). Thus, the presence of phenols and flavonoids in the extract and fractions of *A. melegueta* is a pointer that they could serve as neuroprotectant and neurotherapeutic agents.

Undoubtedly, the quest to discover natural antioxidants is experiencing a renaissance, largely because oxidative stress is strongly linked to the etiology and pathogenesis of many chronic illnesses, including AD (Franceschi et al., 2018). Hence, searching for active AD phytotherapy with antioxidant effects has attracted scientific interest. Herein, the results of the antioxidant actions of the extract and fractions of *A. melegueta* revealed that the extract and fractions had good antioxidant potentials (Figs. 2 and 3). Invariably, scavenging of DPPH and NO is a pointer that the electron/hydrogen-rich phytocompounds present in the extract and fractions donated electrons or hydrogen required to decolorize DPPH radical (purple) to diphenyl picryl hydrazine (yellow) and also might have competed with oxygen thereby decreasing the production of nitrite ions quantified in NO assay (Elufioye et al., 2019).

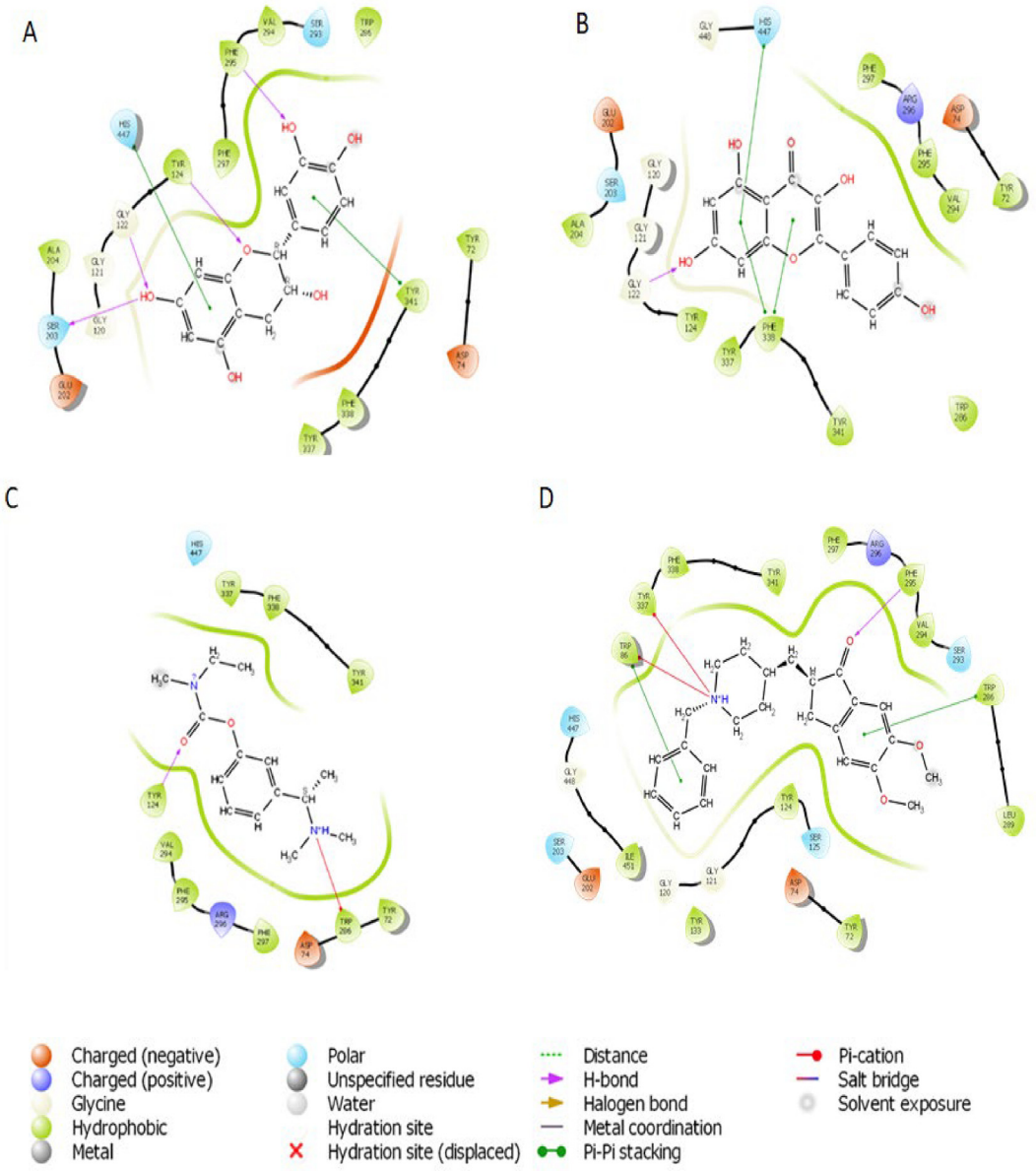

Fig. 8B 2D representation of the interaction between atoms of top-scoring phytocompounds (A), catechin (B), kaempferol (C) Standard drug- Rivastigmine (D) Co-crystalized ligand and amino acids residues of the binding pocket of acetylcholinesterase (4EY7).

Furthermore, the decrease in lipid peroxidation end product (TBARS) and an increase in ferric reducing power of the extract and fractions suggests that they prevented excessive peroxidation of free fatty acids which is an indicator that it could prevent neuronal damages and dysfunction by terminating peroxidation of the high polyunsaturated fatty acids abundance in the brain (Ogunro et al., 2022). Ultimately these antioxidant effects will reduce the presence of lipid peroxides associated with the development of neurofibrillary tangles and senile plaques and also inhibit oxidative stress in the frontal cortex, a major prejorative factor for cognitive impairment (Ege and Şelimen, 2021). Ideally, this remarkable antioxidant potential could be due to the high availability of polyphenols (phenols and flavonoids) in the seeds. Polyphenols donate electrons and hydrogen atoms from their multiple phenol moiety, with subsequent delocalization of the aromatic ring electrons to maintain resonance stability (Caruso et al., 2022; Chukwuma et al., 2020; Onyesife et al., 2023). Collectively, the antioxidant activity was higher in the ethylacetate fraction, followed by the n-hexane fraction, as revealed from their overall IC_{50} values of 102.49 and 115.39 µg/mL respectively (Table 2). Remarkably, their good antioxidant capacity places them as lead agents for maintaining the redox state within the normal physiological range paramount for neuroprotection against AD.

Several clinical and research studies have reported that the pharmaceutical action of acetylcholine is affected by AChE and, to a lesser extent, by BuChE (Khan et al., 2018). However, Inhibition of only AChE will switch compensation mechanisms which will increase the enzymatic activity of BuChE (Elufioye et al., 2019). Hence, compounds that regulate both enzymes are upheld as treatment regimens for AD. Therefore

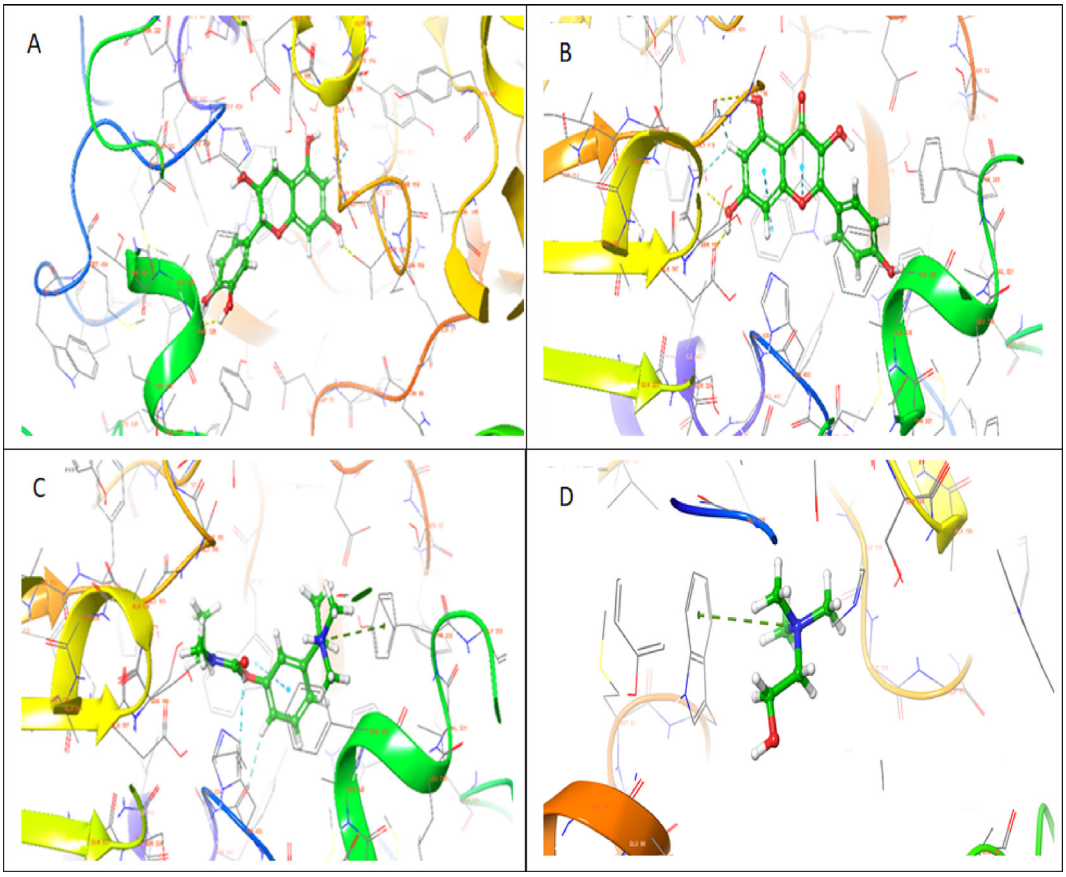

Fig. 9A 3D representation of molecular docking poses of selected compounds (A), catechin (B), kaempferol (C) Standard drug-Rivastigmine (D) Co-crystalized ligand in the binding pocket of butyrylcholinesterase (1P0M).

to provide a comprehensive scientific basis, this study investigated the inhibitory effects of n-hexane and ethylacetate fractions on both AChE and BuChE. Interestingly, both fractions demonstrated good anti-AChE and BuChE effects though the ethylacetate fraction was more potent in both assays. This finding gives evidence that the plant has pharmacologically active phytoconstituents for AD. Furthermore, it is worth noting that inhibition of AChE and BuChE by the fractions will translate to an increase in acetylcholine and butyrylcholine levels which will enhance memory and cognitive function in AD patients, a finding which corroborates with previous pharmacological actions of some natural products (Elufioye et al., 2019). Although, the mechanisms of actions of the anti-AChE effect of the ethylacetate fraction were not studied. According to the structural activity relationship studies of (Khan et al., (2018), flavonoids present in high amount in the fraction show maximal AChE activity due to the position and presence of hydroxyl groups at ring A and B as well as unsaturated ring C, which helps them to exhibit strong hydrogen bond interactions with the essential amino acids of AChE via acting as competitive inhibitors thereby preventing binding of acetylcholine and its subsequent hydrolysis to acetyl and choline groups by AChE and BuChE. Most strikingly, flavonoids' antioxidants and anti-inflammatory activities will provide a multimodal mechanism of action to avert acetylcholine depletion at the synaptic cleft.

Interestingly, several compounds identified in the ethylacetate fraction have been established as neuroprotective agents. Specifically, the potential of flavonoids found in the fraction, including kaempferol, flavanones, anthocyanin, catechin, proanthocyanidin, and naringenin in preventing/or counteracting the progression of neurodegenerative diseases, have been overwhelmingly reported in previous studies (Ali et al., 2018; Mattioli et al., 2020). For instance, positive activities of kaempferol as inhibitors of AChE and BuChE have been established. Szwajgier et al., (2020) reported that kaempferol exerts anti-AChE actions by binding and interacting with the active site amino acids residues (e.g., Asp74, Phe295, or Ser293) of human AChE. Moreso, *in vitro* and *in vivo* reports has shown that kaempferol is effective in suppressing fibrillar β-amyloid deposits formation, expression of COX-2, TNF-a, IL-1B, INOS as well as eliciting increase in the endogenous antioxidants (SOD and GSH) which will orchestrate oxidative damage and neuronal inflammation common in AD patients (Silva dos Santos et al., 2021; Szwajgier et al., 2020). According to Kent et al., (2017), flavanones and anthocyanins are beneficial flavonoids that offer neuroprotection. Myriad of research outcomes have also shown that anthocyanins improve memory and learning via suppressing neuroinflammation, protecting against oxidative damages in neurons, activating nuclear factor erythroid 2–related factor 2 (Nrf2) to enhance endogenous antioxidant synthesis, and modulating cell signal-

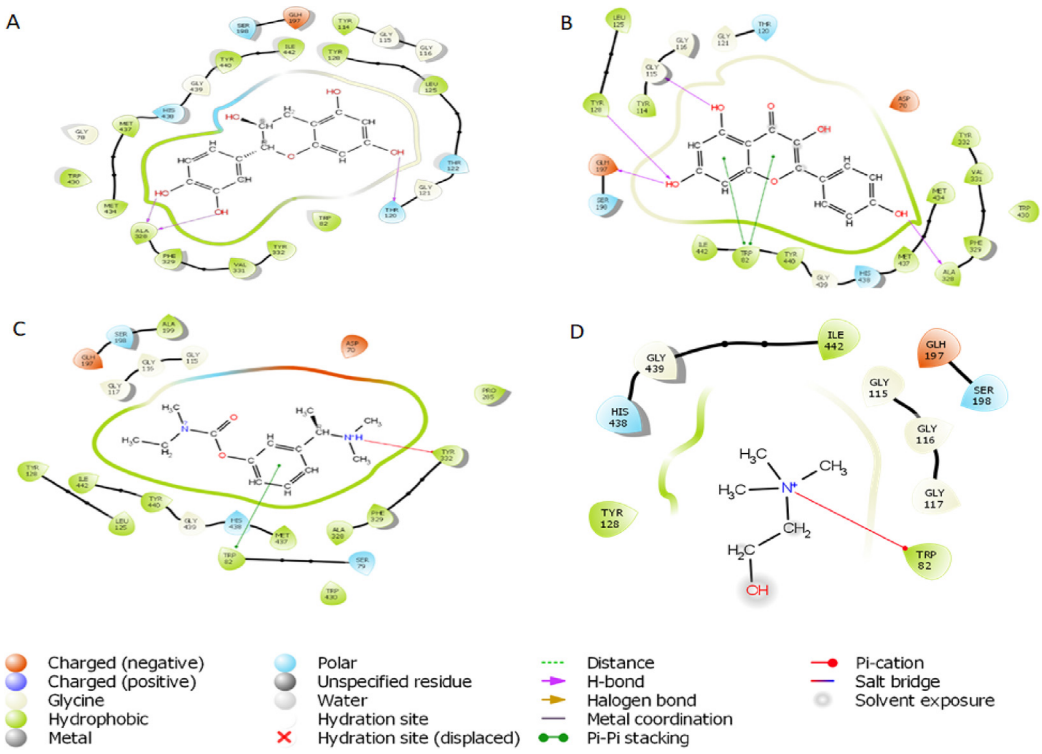

Fig. 9B 2D representation of the interaction between atoms of top-scoring phytocompounds (A), catechin (B), kaempferol (C) and standard drug- Rivastigmine (D) Co-crystallized ligand and amino acids residues of the binding pocket of butyrylcholinesterase (1P0M).

Table 5 MM-GBSA Calculation of Binding free energy (Kcal/mol) for top-ranked ligands in the binding pocket of Acetylcholinesterase (4EY7) and Butyrl Cholinesterase (1P0M).

Top-ranked ligands	Acetylcholinesterase (4EY7)			Butyrl Cholinesterase (1P0M)		
	MMGBSA dG_{bind}	Ligand Energy	Complex Energy	MMGBSA dG_{bind}	Ligand Energy	Complex Energy
Catechin	−51.17	−61.5727	−21483.2	−32.66	−58.7385	−21459.8
Kaemferol	−37.69	−227.108	−21635.2	−36.26	−222.574	−21627.2
Rivastigmine	−57.82	−24.14988	−21404.1	−33.59	−23.47577	−21378.5

ing pathways, notably phosphatidyl-inositol-3-kinase/ AKT pathways (Ali et al., 2018; Mattioli et al., 2020). Most importantly, Mattioli et al., (2020) reported that anthocyanins could protect the brain against neuroinflammation and act as inhibitors of AChE activity by reducing Aβ toxicity in the brain which provokes a decrease in AChE. Moreso, catechin, improves the cognitive function in AD via inhibiting GSK-3β and β, γ-secretase activities thereby preventing neurofibrillary tangles formation and amyloid plaques together with oxidative stress and neuroinflammation (Afzal et al., 2022). Dihydrocytisine, aphyllidine, ephedrine, ribalinidine, and ammodendrine are the alkaloids identified in the fraction. Alkaloids attenuates the development of neurological diseases via inhibiting the activity of AChE, increasing the level of gamma-aminobutyric acid while decreasing oxidative stress and release of neurotoxic inflammatory mediators (Hussain et al., 2018).

Molecular docking saves the failure rate, cost, and time spent in drug discovery and development by determining the interaction of ligands within the target binding cavity with high precision (Apeh et al., 2022; Chukwuma et al., 2022; Onikanni et al., 2021). Interestingly, the top-scoring ligands (catechin, and kaempferol) from our study established favorable interactions in the binding cavities of AChE and BuChE with docking scores in the range of −9.215 to −10.78 and −9.813 to −10.29 kcal/mol, respectively. Comparatively, the docking scores of the ligands were much better than −7.45 and −8.449 Kcal/ obtained in rivastigmine for AChE and BuChE, respectively. The Human AChE active site comprises catalytic site amino acid residues (Ser 203, Glu334, and His447), acyl-binding pocket ((Phe295and Phe297), oxyanion hole at the base of the gorge (Gly120, Gly121, and Ala204), the quaternary ammonium binding locus (Trp86) and finally, PAS consisting of Tyr72, Asp74, Tyr124, Trp286, and Tyr341 which clusters around the entry of the active site gorge (Kumar et al., 2017). It is worth noting that the hydroxyl group found in the catechin ring formed hydrogen bond interactions with SER 203 found in the catalytic site, PHE 295 in

Table 6 ADMET prediction output of test compounds.

Parameters	Catechin	Kaempferol	Rivastigmine
Druglikeness			
Molecular weight (g/mol)	290.26	286.24	250.34
Nrot	1	1	6
iLog P	1.47	1.70	3.21
# HBA	6	6	3
# HBD	5	4	0
Molar reactivity	74.33	76.01	73.12
TPSA ($A^{2)}$)	110.38	111.13	32.78
Lipinski violations	0	0	0
Veber violations	0	0	0
Pharmacokinetics			
Bioavailability score	0.55	0.55	0.55
GI absorption	High	High	High
BBB permeant	No	No	Yes
P-gp substrate	Yes	No	No
CYP1A2 inhibitor	No	Yes	No
CYP2C19 inhibitor	No	No	No
CYP2C9 inhibitor	No	No	No
CYP2D6 inhibitor	No	Yes	No
CYP3A4 inhibitor	No	Yes	No
Log K_p (cm/s) (skin permeation)	−7.82	−6.70	−6.2
Toxicity			
Predicted LD_{50} (mg/kg)	10,000	3919	1,000
Predicted toxicity class	6	5	4
Hepatotoxicity	−	−	−
Carcinogenicity	−	−	−
Immunogenicity	−	−	+
Mutagenicity	−	−	−
Cytotoxicity	−	−	−

Key: #HBD: No of hydrogen bond donor, #HBA: No of hydrogen bond acceptors, Log P; octanol–water partition coefficient, TPSA; topological polar surface area, Nrot; # rotatable hydrogen bond, GIA; gastrointestinal absorption, BBB; blood–brain barrier, Pgp; P-glycoprotein, CYP450; Cytochrome P450, Log kp; skin permeation, LD_{50}: lethal median dose, + Active, − inactive.

the acyl-binding pocket, TYR 124 in the PAS while having pi-pi interactions with HIS 447 located at catalytic site and TYR 341 in the PAS residue. Also, kaempferol established a hydrogen bond with GLY 122 close to the oxyanion hole at the base of the gorge and pi-pi stacking interactions with the catalytic site HIS 447. However, the standard inhibitor, rivastigmine, formed a hydrogen bond with TYR 124 and Pi-cation with TRP 286, which are all PAS amino acids residue. The co-crystallized ligand had pi –cation (TYR337, TRP86), H-bond (PHE295) and pi-pi (TRP86,TRP286) interactions with amino acids residues of AChE. According to Kumar et al., (2017), the human BuChE active site is made up of the catalytic site (Ser198, His438, and Glu325), the cation-π site or choline-binding site (Trp82), the acyl binding site (Leu286, Val288), oxyanion hole (Gly116, Gly117, Ala199), and PAS (Asp70). Herein, kaempferol formed a hydrogen bond with GLY115 close to the oxyanion hole using hydroxyl group found on its phenolic ring as well as two pi-pi stacking with TRP82 while the co-crystallized ligand had pi-cation interaction with TRP82 (Table 4). Hydrogen bonds and pi-pi stacking interactions helps in stabilizing the structures of bio-molecules, enzyme catalysis, and stability of ligand–protein complex (Kikiowo et al., 2020). Thus, interactions of our ligands with the active sites' amino acids residues which will inhibit binding and subsequent hydrolysis of the primary substrate, acetylcholine, into acetic acid and choline, will improve cholinergic transmission and cognitive function in AD patients. Similarly, MM-GBSA calculated binding free energy also revealed that the hits had high binding energy. Several studies have reported that the binding free energy estimated from an accurately docked complex is very similar to experimentally determined activities (Chukwuma et al., 2022; Kikiowo et al., 2020; Maffucci et al., 2018; Tripathi et al., 2013). Therefore, from all the binding energies (Table 5), it can be deduced that all our hit compounds showed interesting stabilities in the binding pockets of both AChE and BChE.

ADMET prediction uses in silico approach to investigate whether a drug candidate will be quickly and easily absorbed, distributed to its specific site of action, metabolized favorably, and eliminated from the body without eliciting any toxic side effects (Johnson et al., 2022). The hits, catechin, and kaempferol obeyed the drug-likeness rule for being an orally active drug as shown by their zero violation of Lipinski (Molecular weight $\leq$ 500, hydrogen bond acceptor $\leq$ 10 (count of O and N atoms), hydrogen bond donor $\leq$ 5 (count of OH and NH groups) and Log P $\leq$ 5) (Lipinski et al 2004) and Veber rules (Nrot $<$ 5and TPSA $\leq$ 140 A^2) (Table 6). This was validated by their bioavailability score (BAS) of 0.55 and high gastrointestinal absorption. Potential drug candidates that obey drug-likeness rules tend to have a lower attrition rate in phases I, II, and III of the clinical trial (Kikiowo et al., 2020). Also, their BAS (0.55%) is a pointer that the compounds have about a 55% probability of a minimum of 10% oral absorption (Johnson et al., 2022). Although kaempferol and catechin were predicted not to have BBB permeation, they could also gain access to the brain through the hypophysis, area postrema, median eminence, paraphysis, preoptic recess, pineal gland, and choroid plexus endothelium where BBB is absent to exert their neurotherapeutic effects (DosSantos et al., 2014). In addition, AD-induced tissue damage leads to the release of signaling molecules such as IL-1B, TNF-α serotonin, and histamine, which disrupt the functions and morphology of the transmembrane proteins mediating BBB (DosSantos et al., 2014). This is in tandem with the study of Rangel-Ordóñez et al., (2010) who proved from their *in vivo* studies that kaempferol is widely distributed in the striatum, hippocampus, and frontal cortex, where damage occurs during the early stages of AD. Likewise, transformation of absorbed catechin in the small intestine by enterocytes forms conjugated eleven catechin ring fission products which could cross the BBB to reach brain parenchyma where it promotes neuritogenesis which ultimately reduces neurodegeneration (Pervin et al., 2019). To add credence to this, Afzal et al., 2022 reported that in several human studies, catechin was found to decreases oxidative stress, lipid peroxidation, increase acetylcholine level and prevalence of cognitive impairment in AD patients. Furthermore, the none inhibitory effects of all the selected compounds on cytochrome P450 isoforms CYP450 2C19 and 2C9 oxidases required to mediate the plasma concentration of drugs suggest that they may not likely induce toxicity as a result of drug-drug interactions (Chukwuma et al., 2022; Da Rocha et al., 2022). This concurs with the predicted toxicity profile, which revealed that catechin, and kaempferol are not likely hepatotoxic, carcinogenic,

immunogenic, mutagenic, and cytotoxic when compared side by side with rivastigmine which is immunogenic thereby placing them as a safe drug for AD.

5. Conclusions

Based on the findings from this bioassay-guided study, *A. melegueta* seeds extract/fractions have good antioxidant and anti-cholinesterase activity which was optimal in the ethylacetate fraction. Furthermore, GC-FID screening of the fraction revealed that it is kaempferol rich and had an abundance of other phytoconstituents. Again, the high docking scores, favorable interactions with active site amino acids residue of AChE and BuChE, and high binding energy of the top scoring compounds (catechin, and kaempferol) show that they could be better inhibitors of AChE and BuChE enzymatic activities than the reference drug, rivastigmine. Moreso, the compounds' established drug-likeness and safety profile position them as effective and safe targets. Thus, they could be employed as therapeutic drug candidates for treating and managing AD. However, further *in vivo* studies and clinical trials could further be used to attest to the effects.

Declaration of Competing Interest

The authors declare that they have no known competing financial interests or personal relationships that could have appeared to influence the work reported in this paper.

Acknowledgements

This study is supported via funding from Prince Sattam bin Abdulaziz University project number (PSAU/2023/R/1444).

Appendix A. Supplementary material

Supplementary data to this article can be found online at https://doi.org/10.1016/j.arabjc.2023.105089.

References

Abdou, R.M., El-Maadawy, W.H., Hassan, M., El-Dine, R.S., Aboushousha, T., El-Tanbouly, N.D., El-Sayed, A.M., 2021. Nephroprotective activity of Aframomum melegueta seeds extract against diclofenac-induced acute kidney injury: A mechanistic study. J. Ethnopharmacol. 273, 113939.

Afzal, O., Dalhat, M.H., Altamimi, A.S.A., Rasool, R., Alzarea, S.I., Almalki, W.H., Murtaza, B.N., Iftikhar, S., Nadeem, S., Nadeem, M.S., Kazmi, I., 2022. Green tea catechins attenuate neurodegenerative diseases and cognitive deficits. Molecules 27, 7604–7625.

Ali, T., Kim, T., Rehman, S.U., Khan, M.S., Amin, F.U., Khan, M., Ikram, M., Kim, M.O., 2018. Natural dietary supplementation of anthocyanins via PI3K/Akt/Nrf2/HO-1 pathways mitigate oxidative stress, neurodegeneration, and memory impairment in a mouse model of alzheimer's disease. Mol. Neurobiol. 55, 6076–6093.

Alothaid, H., 2022. Evaluation of cytotoxicity, oxidative stress and organ-specific effects of activated carbon from Al-Baha date palm kernels. Saudi J. Biol. Sci. 29,. https://doi.org/10.1016/j.sjbs.2022.103387 103387.

Apeh, V.O., Njoku, O.U., Nwodo, F.O.C., Chukwuma, I.F., Emmanuel, A.A., 2022. In silico drug-like properties prediction and in vivo antifungal potentials of Citrullus lanatus seed oil against Candida albicans. Arab. J. Chem. 15,. https://doi.org/10.1016/j.arabjc.2021.103578 103578.

Awan, S.S., Khan, T.R., Mehmood, A., Hafeez, M., Abass, Rizwan, S., Nazir, M., Raffi, M., 2023. Ailanthus altissima leaf extract mediated green production of zinc oxide (ZnO) nanoparticles for antibacterial and antioxidant activity. Saudi J. Biol. Sci. 30,. https://doi.org/10.1016/j.sjbs.2022.103487 103487.

Ayaz, M., Sadiq, A., Junaid, M., Ullah, F., Ovais, M., Ullah, I., Ahmed, J., Shahid, M., Gris, D., 2019. Flavonoids as prospective neuroprotectants and their therapeutic propensity in aging associated neurological disorders. Front. Aging Neurosci. 11, 155. https://doi.org/10.3389/fnagi.2019.00155.

Ayaz, M., Nawaz, A., Naz, F., Ullah, F., Sadiq, A., Islam, Z.U., 2022. Phytochemicals-based therapeutics against Alzheimer's Disease: an update. Curr. Top. Med. Chem. 22, 1811–1820. https://doi.org/10.2174/1568026622666220815104305.

Banerjee, A., Dasgupta, N., De, B., 2005. In vitro study of antioxidant activity of Syzygium cumini fruit. Food Chem 90, 727–733. https://doi.org/10.1016/j.foodchem.2004.04.033.

Capatina, L., Todirascu-Ciornea, E., Napoli, E.M., Ruberto, G., Hritcu, L., Dumitru, G., 2020. Thymus vulgaris essential oil protects zebrafish against cognitive dysfunction by regulating cholinergic and antioxidants systems. Antioxidants 9, 1–18. https://doi.org/10.3390/antiox9111083.

Caruso, G., Godos, J., Privitera, A., Lanza, G., Castellano, S., Chillemi, A., Bruni, O., Ferri, R., Caraci, F., Grosso, G., 2022. Phenolic acids and prevention of cognitive decline: polyphenols with a neuroprotective role in cognitive disorders and Alzheimer's disease. Nutrients 14, 819–853. https://doi.org/10.3390/nu14040819.

Chukwuma, I.F., Nkwocha, C.C., Ezeanyika, L.U.S., Ogugua, V.N., 2020. Phytochemical investigation and in vitro antioxidant potency of root bark of brenania brieyi fractions. Trop. J. Nat. Prod. Res. 4, 970–975. https://doi.org/10.26538/tjnpr/v4i11.21.

Chukwuma, I.F., Nworah, F.N., Apeh, V.O., Omeje, K.O., Nweze, E. J., Asogwa, C.D., Prince, T., Ezeorba, C., 2022. phytochemical characterization, functional nutrition, and anti-diabetic potentials of Leptadenia hastata (per) decne leaves . In silico and in vitro studies. Bioinform. Biol. Insights 16, 1–17. https://doi.org/10.1177/11779322221115436.

Chukwuma, I.F., Apeh, V.O., Nwora, F.N., Nkwocha, C.C., Mba, S. E., Ossai, E.C., 2023. Phytochemical profiling and antioxidative potential of phenolic-rich extract of cola acuminata nuts. Biointerface Res. Appl. Chem. 13, 29–39.

Da Rocha, M.N., Marinho, E.S., Marinho, M.M., Dos Santos, H.S., 2022. Virtual screening in pharmacokinetics, bioactivity, and toxicity of the amburana cearensis secondary metabolites. Biointerface Res. Appl. Chem. 12, 8471–8491. https://doi.org/10.33263/BRIAC126.84718491.

Dos Santos, T.C., Gomes, T.M., Pinto, B.A.S., Camara, A.L., De Andrade Paes, A.M., 2018. Naturally occurring acetylcholinesterase inhibitors and their potential use for Alzheimer's disease therapy. Front. Pharmacol. 9, 1192. https://doi.org/10.3389/fphar.2018.01192.

DosSantos, M.F., Holanda-Afonso, R.C., Lima, R.L., DaSilva, A.F., Moura-Neto, V., 2014. The role of the blood–brain barrier in the development and treatment of migraine and other pain disorders. Front. Cell. Neurosci. 8, 1–14. https://doi.org/10.3389/fncel.2014.00302.

Ege, T., Şelimen, H.D., 2021. Monoamine oxidase inhibitory effects of medicinal plants in management of Alzheimer's disease. J. Turkish Chem. Soc. Sect. A Chem. 8, 239–248. https://doi.org/10.18596/jotcsa.823874.

El-Kelawy, H.M., Mansour, M.A., El-Naggar, R.E., Nabila, E., Elkassas, E., 2017. Effect of garlic (allium sativum) treatment on hematological, biochemical, hormonal and fertility parameters of male bouscat rabbits. Egypt. J. Rabbit Sci. 27, 341–358.

Ellman, G.L., Courtney, K., Andres, V., Featherstone, R.M., 1961. A new and rapid colorimetric determination of acetylcholinesterase activity. Biochem. Pharmacol. 7, 88–95.

Elufioye, T.O., Chinaka, C.G., Oyedeji, A.O., 2019. Antioxidant and anticholinesterase activities of macrosphyra Longistyla D) Hiern relevant in the management of Alzheimer' s disease. Antioxidants 8, 400–414. https://doi.org/10.3390/antiox8090400.

Franceschi, C., Garagnani, P., Morsiani, C., Conte, M., Santoro, A., Grignolio, A., Monti, D., Capri, M., Salvioli, S., 2018. The continuum of aging and age-related diseases : common mechanisms but different rates. Front. Med. 5, 61. https://doi.org/10.3389/fmed.2018.00061.

Gyamfi, M.A., Yonamine, M., Aniya, Y., 1999. Free radical scavenging action of medical herbs from Ghana : Thonningia sanguinea on experimentally induced liver injuries. Gen. Pharmacol. 32, 661–667. https://doi.org/10.1016/s0306-3623(98)00238-9.

Hampel, H., Hardy, J., Blennow, K., Chen, C., Perry, G., Kim, S.H., Villemagne, V.L., Aisen, P., Vendruscolo, M., Iwatsubo, T., Masters, C.L., Cho, M., Lannfelt, L., Cummings, J.L., Vergallo, A., 2021. The Amyloid-β Pathway in Alzheimer's Disease. Mol. Psychiatry 26, 5481–5503. https://doi.org/10.1038/s41380-021-01249-0.

Hussain, G., Rasul, A., Anwar, H., Aziz, N., Razzaq, A., Wei, W., Ali, M., Li, J., Li, X., 2018. Role of plant derived alkaloids and their mechanism in neurodegenerative disorders. Int. J. Biol. Sci. 14, 341–357. https://doi.org/10.7150/ijbs.23247.

Johnson, T.O., Adegboyega, A.E., Ojo, O.A., Yusuf, A.J., Iwaloye, O., Ugwah-Oguejiofor, C.J., Asomadu, R.O., Chukwuma, I.F., Ejembi, S.A., Ugwuja, E.I., Alotaibi, S.S., Albogami, S.M., Batiha, G.-S., Rajab, B.S., Conte-Junior, C.A., 2022. A computational approach to elucidate the interactions of chemicals from Artemisia annua targeted toward SARS-CoV-2 main protease inhibition for COVID-19 treatment. Front. Med. 9,. https://doi.org/10.3389/fmed.2022.907583 907583.

Kent, K., Charlton, K., Roodenrys, S., Batterham, M., Potter, J., Traynor, V., Gilbert, H., Morgan, O., Richards, R., 2017. Consumption of anthocyanin-rich cherry juice for 12 weeks improves memory and cognition in older adults with mild-to-moderate dementia. Eur. J. Nutr. 56, 333–341. https://doi.org/10.1007/s00394-015-1083-y.

Khan, H., Amin, S., Ajmal, M., Patel, S., 2018. Biomedicine & Pharmacotherapy Flavonoids as acetylcholinesterase inhibitors : Current therapeutic standing and future prospects. Biomed. Pharmacother. 101, 860–870. https://doi.org/10.1016/j.biopha.2018.03.007.

Kikiowo, B., Ogunleye, J.A., Iwaloye, O., Ijatuyi, T.T., 2020. Therapeutic potential of Chromolaena odorata phyto-constituents against human pancreatic α-amylase. J. Biomol. Struct. Dyn. https://doi.org/10.1080/07391102.2020.1833758.

Kpemissi, M., Kantati, Y.T., Veerapur, V.P., Eklu-Gadegbeku, K., Hassan, Z., 2023. Anti-cholinesterase, anti-inflammatory and antioxidant properties of Combretum micranthum G. Don: Potential implications in neurodegenerative disease. IBRO Neurosci. Reports 14, 21–27. https://doi.org/10.1016/j.ibneur.2022.12.001.

Kumar, S., Chowdhury, S., Kumar, S., 2017. In silico repurposing of antipsychotic drugs for Alzheimer's disease. BMC Neurosci. 18, 1–16. https://doi.org/10.1186/s12868-017-0394-8.

Maffucci, I., Hu, X., Fumagalli, V., Contini, A., 2018. An efficient implementation of the Nwat-MMGBSA method to rescore docking results in medium-throughput virtual screenings. Front. Chem 6, 43. https://doi.org/10.3389/FCHEM.2018.00043/BIBTEX.

Mangmool, S., Kunpukpong, I., Kitphati, W., Anantachoke, N., 2021. Antioxidant and anticholinesterase activities of extracts and phytochemicals of syzygium antisepticum leaves. Molecules 26, 3295–3309. https://doi.org/10.3390/molecules26113295.

Mattioli, R., Francioso, A., Mosca, L., Silva, P., 2020. Anthocyanins : A comprehensive review of their chemical properties and health effects on cardiovascular and neurodegenerative diseases. Molecules 25, 3809–3850. https://doi.org/10.3390/molecules25173809.

Nkwocha, C.C., Ogugofor, M.O., Chukwuma, I.F., Njoku, O.U., 2022. Identification and characterization of phytochemicals and constituents in Desmodium velutinum stem using high-performance liquid chromatography (HPLC). Pharmacol. Res. - Mod. Chinese Med. 3,. https://doi.org/10.1016/j.prmcm.2022.100090 100090.

Ogunro, O.B., Salawu, A.O., Alotaibi, S.S., Albogami, S.M., Batiha, G.E.S., Waard, M.D., 2022. Quercetin-3-O-β-D-glucopyranoside-rich fraction from spondias mombin leaves halted responses from oxidative stress, Neuroinflammation, apoptosis, and lipid peroxidation in the brain of Dichlorvos-treated wistar rats. Toxics 10. https://doi.org/10.3390/toxics10080477.

Ojo, O.A., Ojo, A.B., Okolie, C., Abdurrahman, J., Barnabas, M., Evbuomwan, I.O., Atunwa, O.P., Atunwa, B., Iyobhebhe, M., Elebiyo, T.C., Nwonuma, C.O., Adegboyega, A.E., Qusti, S., Alshammari, E.M., Hetta, H.F., Batiha, G.E.S., 2021a. Elucidating the interactions of compounds identified from Aframomum melegueta seeds as promising candidates for the management of diabetes mellitus: A computational approach. Informatics Med. Unlocked 26,. https://doi.org/10.1016/j.imu.2021.100720 100720.

Ojo, O.A., Ojo, A.B., Okolie, C., Nwakama, M.A.C., Iyobhebhe, M., Evbuomwan, I.O., Nwonuma, C.O., Maimako, R.F., Adegboyega, A.E., Taiwo, O.A., Alsharif, K.F., Batiha, G.E.S., 2021b. Deciphering the interactions of bioactive compounds in selected traditional medicinal plants against alzheimer's diseases via pharmacophore modeling, auto-QSAR, and molecular docking approaches. Molecules 26, 1996–2020. https://doi.org/10.3390/molecules26071996.

Onikanni, A.S., Lawal, B., Olusola, A.O., Olugbodi, J.O., Sani, S., Ajiboye, B.O., Ilesanmi, O.B., Alqarni, M., Mostafahedeab, G., Obaidullah, A.J., Batiha, G.E.S., Wu, A.T.H., 2021. Sterculia tragacantha Lindl Leaf Extract Ameliorates STZ-Induced Diabetes, Oxidative Stress, Inflammation and Neuronal Impairment. J. Inflamm. Res. 14, 6749–6764. https://doi.org/10.2147/JIR.S319673.

Onyesife, O.C., Cukwuma, I.F., Okagu, I.U., Ndefo, C.J., Amujiri, A. N., Ogugua, V.N., 2023. Nephroprotective effects of Piper nigrum extracts against monosodium glutamate-induced renal toxicity in rats. Sci. African 19, e01453.

Oyaizu, M., 1986. Studies on products of browning reactions: antioxidant activities of products of browning reaction prepared from glucosamine. JPN J. Nutr. 44, 307–315.

Pervin, M., Unno, K., Takagaki, A., Isemura, M., Nakamura, Y., 2019. Function of Green tea catechins in the brain: epigallocatechin gallate and its metabolites. Int. J. Mol. Sci. 20, 3630.

Phanrang, P.T., Baruah, P., Chandra, A.K., Mitra, S., 2022. Auxiliary therapeutic role of cholinergic agents: mechanistic insights into the antioxidant behavior of Alzheimer's disease drugs. J. Phys. Chem. A 126, 546–556. https://doi.org/10.1021/acs.jpca.1c09146.

Rangel-Ordóñez, L., Nöldner, M., Schubert-Zsilavecz, M., Wurglics, M., 2010. Plasma levels and distribution of flavonoids in rat brain after single and repeated doses of standardized Ginkgo biloba extract EGb 761®. Planta Med. 76, 1683–1690. https://doi.org/10.1055/s-0030-1249962.

Silva dos Santos, J., Gonçalves Cirino, J.P., de Oliveira Carvalho, P., Ortega, M.M., 2021. The pharmacological action of kaempferol in central nervous system diseases: A review. Front. Pharmacol. 11,. https://doi.org/10.3389/fphar.2020.565700 565700.

Silva, R.F.M., Pogačnik, L., 2020. Polyphenols from food and natural products: Neuroprotection and safety. Antioxidants 9, 61–73. https://doi.org/10.3390/antiox9010061.

Singleton, V.L., Rossi, J.A., 1965. Colorimetric of total phenolics with phosphomolybdic-phosphotungstic acid reagents. Am. J. Enol. Vinic. 16, 144–158.

Sreejayan, N., Rao, M.N.A., 1997. Nitric oxide scavenging by curcuminoids. J. Pharm. Pharmacol. 49, 105–107.

Szwajgier, D., Borowiec, K., Zapp, J., 2020. Activity-guided isolation of cholinesterase inhibitors quercetin, rutin and kaempferol from Prunus persica fruit. Zeitschrift fur Naturforsch. - Sect C. J. Biosci. 75, 87–96. https://doi.org/10.1515/znc-2019-0079.

Tönnies, E., Trushina, E., 2017. Oxidative stress, synaptic dysfunction, and Alzheimer's disease. J. Alzheimer's Dis. 57, 1105–1121. https://doi.org/10.3233/JAD-161088.

Tripathi, S.K., Muttineni, R., Singh, S.K., 2013. Extra precision docking, free energy calculation and molecular dynamics simulation studies of CDK2 inhibitors. J. Theor. Biol. 334, 87–100. https://doi.org/10.1016/J.JTBI.2013.05.014.

Tysoe, C.R., Caner, S., Calvert, M.B., Win-Mason, A., Brayer, G.D., Withers, S.G., 2019. Synthesis of montbretin A analogues yields potent competitive inhibitors of human pancreatic α-amylase. Chem. Sci. 10, 11073–11077. https://doi.org/10.1039/C9SC02610J.

Zhishen, J., Mengcheng, T., Jianming, W., 1999. The determination of flavonoid contents in mulberry and their scavenging effects on superoxide radicals. Food Chem. 64, 555–559. https://doi.org/10.1016/S0308-8146(98)00102-2.